Frontiers in Heat and Mass Transfer

Tech Science Press

DOI: 10.32604/fhmt.2024.056779

ARTICLE

The Hydrodynamic Crisis of Nucleate Boiling in a Horizontal Thin Layer of Dielectric Liquid HFE-7100

V. I. Zhukov[1,2,*] and A. N. Pavlenko[1]

[1]Kutateladze Institute of Thermophysics, Siberian Branch, Russian Academy of Sciences, Novosibirsk, 630090, Russia

[2]Department of Chemistry and Chemical Technology, Novosibirsk State Technical University, Novosibirsk, 630073, Russia

*Corresponding Author: V. I. Zhukov. Email: v.zhukov@corp.nstu.ru

Received: 30 July 2024 Accepted: 16 October 2024 Published: 19 December 2024

ABSTRACT

The results of an experimental study on critical heat fluxes (CHF) during the nucleate boiling of the HFE-7100 dielectric liquid in horizontal layers of different heights at atmospheric pressure are presented. The existence of a critical layer height has been established. In layers above the critical layer height, a hydrodynamic boiling crisis occurs; in thinner layers, a surface drying crisis occurs. At a layer height equal to the critical value, a dry spot first appears, followed by transition boiling, which gradually spreads to the entire heating surface. In these experiments, the critical layer height was equal to 6 mm. In a layer of liquid with a critical layer height of 6 mm, a two-dimensional Taylor instability was observed in the transition boiling mode when the ratio of the diameter of the "vapor jets" to the distance between them, as well as the void fractions in the layer ($\sim\pi/16$), corresponded to the main provisions of the Zuber theory. The calculation of CHF using the relations of Zuber's theory, when approaching the crisis from the transition boiling side and taking into account the real geometric dimensions, aligns well with the experimental results.

KEYWORDS

Boiling; instabilities; critical heat flux; horizontal liquid film

Nomenclature

Symbols

A	Area, m^2
d	Diameter, m
g	Acceleration of gravity, m/s^2
h	Initial layer height, m
h_{LG}	Latent heat of vaporization, J/kg
k	Kutateladze constant
l_v	Distance between the centers of "vapor jets", mm
$l_\sigma = (\sigma/g(\rho_l - \rho_v))^{1/2}$	Laplace constant, m
m	Wave number, m^{-1}

q	Heat flux, W/m^2
T	Temperature, °C, K

Greek Symbols

$\lambda_d = 2\pi\sqrt{3}l_\sigma$	Most dangerous wavelength of Taylor instability, m
$\lambda_{cr} = 2\pi l_\sigma$	Critical wavelength of Taylor instability m
ρ	Density, kg/m^3
σ	Surface tension, N/m
τ	Time, s

Subscripts and Superscripts

cr	Critical
Calc	Calculation using parameters taken from experiment
H	Referred to Helmholtz instability
K	Referred to Kutateladze equation
l	Liquid
s	Parameter on saturation line
t	Theoretical values of parameters and calculations using them
v	Vapor
w	Referred to heated surface
Z	Refers to Zuber theory

1 Introduction

Dielectric liquids are used for immersion cooling of micro and power electronic elements [1,2]. The saturation temperature for these liquids at atmospheric pressure is approximately (30–65)°C, with a permissible device heating temperature of approximately 85°C. The critical heat flux (CHF) limits the maximum heat flux that can be removed from the surface of a device as it cools. In works [3–5], a study was carried out on CHF during the pool boiling of the dielectric liquid HFE-7100 on surfaces with different roughness at various pressures. An increase in the CHF with increasing pressure is noted. The results of visual observations of the processes are presented; however, the authors primarily limited themselves to a qualitative description of the observed vapor structures. In [4], a boiling crisis on a copper surface with a diameter of 40 mm was investigated. Photographs of vapor structures at the moment of crisis and during transition boiling are provided. The presence of vapor bubbles of various sizes, vapor columns and mushroom-shaped bubbles is noted. In [5], it is noted that the CHF decreases with decreasing pressure and then increases slightly, i.e., a weak dependence of the CHF on pressure is observed in this range. It is noted that the value of CHF can be affected by the height of the liquid layer. The results of systematic studies on the influence of liquid layer height and reduced pressure over a wide range of variations are presented in [6,7]. In [6], a decrease in the CHF with decreasing pressure was also observed, followed by an increase in the CHF in a thick layer of liquid, when the process patterns were practically no different from those of the pool boiling process. In [8], the influence of the smooth heater size on the value of the CHF and heat transfer coefficients during the pool boiling of FC-72 on eight smooth silicon chips of different sizes is studied. It was found that when the chip side size exceeds $3\lambda_d$ (Comments regarding λ_d are contained in [9,10]), the CHFs do not depend on the heater size and are described by the relationship obtained in [11,12] for the CHF on an infinite plane. The sizes of chips are continuously increasing and have already closely approached the sizes

at which the regularities of the boiling process are described by dependencies typical of heaters of infinite size. Under these conditions, one of the independent parameters influencing the value of the CHF may be the height of the liquid layer. The use of thin liquid layers of optimal height can increase the CHF compared to pool boiling of the liquid and can also significantly reduce the mass and size characteristics of the equipment, as well as the consumption of the coolant. Therefore, studying the CHF value in layers of liquid of different heights is an important research task.

Kutateladze in [13] obtained a relationship for calculating the CHF during nucleate boiling of a liquid on a very large horizontal plate with the heating surface facing upwards, using the method of dimensional analysis:

$$q_{crK} = kh_{LG}\rho_v \left(\frac{\sigma g\,(\rho_l - \rho_v)}{\rho_v^2} \right)^{1/4} \tag{1}$$

where Kutateladze recommended taking $k = 0.16$. Since this equation was derived from dimensional analysis, various theoretical models of CHF for pool boiling can be represented by Eq. (1), regardless of the proposed CHF mechanism.

Zuber in [14,15] obtained an equation for calculating the CHF on an infinite plane. To calculate the CHF, he recommended using $k = 0.131$ in (1). In Zuber's analysis, the right-hand side of Eq. (1) was multiplied by the expression $(\rho_l/(\rho_l + \rho_v))^{1/2}$, which differs significantly from unity only at near-critical pressures. Zuber constructed a CHF model based on the Taylor-Helmholtz theory of hydrodynamic instability between ascending vapor flow and a descending liquid flow. His model contains a developed mathematical apparatus that allows for various improvements and new results. In [16–18], various CHF models for pool boiling are considered, along with evaluations of CHF models and correlations. In [19], a similar approach, as described in [14,15], is used to predict CHF on bifilar surfaces based on Helmholtz instability and Taylor instability.

Lienhard et al. [11,12] applied the Zuber model to calculate the CHF for pool boiling of liquid on geometric bodies of various shapes, such as spheres, cylinders, and vertical plates. They showed that if the size of the horizontal surface is greater than $3\lambda_d$, it can be considered an infinite plane. In [11,12], it was proposed to use the length of the most dangerous wave of Taylor instability as the wavelength of Helmholtz instability $\lambda_H = \lambda_d$ and and it was found that $k = 0.149$, which better matches the experimental data. In the experiments [11,12], the horizontal heating surface was confined by vertical walls to eliminate the lateral inflow of liquid, which has a noticeable effect on the CHF. In [20], the shortcomings of the Zuber model and the difficulties in experimentally verifying of the main postulates are discussed. The relationships between the characteristic geometric dimensions of the vapor jets and their spatial arrangement can be established by analyzing visual observations, which can be very difficult to do when studying a crisis in pool boiling. Therefore, Yagov [21] in 2014 once again repeated the ironic opinion of Bergls [22], expressed in 1992 regarding visual observations of boiling crises in motion pictures and photo frames "One sees what one wants to see to support a particular mechanistic model", which most accurately characterizes the state of research in the field of confirming Zuber's hydrodynamic theory for pool boiling. In Zuber's theory, the void fraction in the near-wall layer of liquid at the beginning of the boiling crisis is equal to $\pi/16$, as noted in [21]. In experiments, however, the void fraction of the wall layer is usually much greater.

Most experiments measuring CHF are performed under pool boiling conditions. More comprehensive requirements for conditions that satisfy the criteria of Zuber's theory were formulated by Theofanus et al. [23,24]. Just as in the experiments [11,12], he says that the cross-section of the liquid volume in the horizontal plane must completely coincide with the cross-section of the heater.

In experimental practice, this means that the heating surface must be limited by vertical walls. It is also necessary for the aspect ratio—the ratio of the thickness of the liquid layer to the smallest lateral dimension of the heating surface—to be small. However, specific recommendations regarding the height of the liquid layer and the ratio of the layer height to the dimensions of the plate are not provided in these works, making it necessary to conduct detailed experiments in this area.

In previous works by the authors of this article [25,26], the distribution of large bubbles in pre-crisis boiling regimes within a liquid layer on a horizontal surface with vertical walls was investigated. The two-dimensional instability of a boiling layer of liquid was experimentally discovered. It is shown in [26] that the distribution of "vapor jets" occurs in accordance with the conclusions of the two-dimensional Taylor instability [27]. The influence of the liquid layer thickness and void fraction in the layer on the mechanism of occurrence of the CHF and its magnitude was studied. The instability wavelength in a boiling liquid layer depends on the void fraction and is proportional to the wavelength of Taylor instability. Using the mathematical apparatus of Zuber's theory, a hydromechanical model of the nucleate boiling crisis is proposed, both when approached from the developed nucleate boiling regime and in the case of a symmetric problem: the calculation of CHF when approached from the transition boiling side. The geometric characteristics of the vapor-liquid layer during transition boiling differ significantly from those proposed in Zuber's theory [14,15]. The "vapor jets" had approximately the same diameter, equal to λ_d, which is 2 times greater than that postulated by Zuber's theory. As a result, the distance between the "vapor jets" in [26] was greater than that in [14,15]. The "vapor jets" uniformly filled the entire heating surface, and the liquid returned to the heating surface along the meniscus between the "vapor jets", while in Zuber's theory, the ascending vapor flow was surrounded by a descending liquid flow. The void fraction in the liquid layer in [26] is estimated to be $\pi/4$, while in Zuber's theory, the void fraction is equal to $\pi/16$. We are not aware of any experimental studies in which the void fraction in the liquid layer is approximately $\pi/16$ when approaching the hydrodynamic crisis from the transition boiling side, and in which the dependence postulated in Zuber's theory between the sizes of the "vapor jets" and the distance between them is observed. The authors of this article [6,7,25] showed that a hydrodynamic boiling crisis occurs in thick liquid layers, while a surface drying crisis is observed in thin liquid layers. Therefore, there is a critical layer height h_{cr}, above which a hydrodynamic boiling crisis is observed, and below which a surface drying crisis occurs. The question arises: what are the features of the hydrodynamic boiling crisis at the layer height h_{cr}?

In this paper, an experimental study of CHF in thin horizontal layers of the dielectric liquid HFE-7100 is performed, depending on changes in a wide range of layer heights at atmospheric pressure. The experimental results are compared with known calculated dependencies. The results of the statistical processing of visual observations and calculations of CHF are presented based on the measurements of the diameters of "vapor jets" and the wavelengths of two-dimensional Taylor instability observed in a layer with a critical height of $h_{\text{cr}} = 6$ mm in the transition boiling mode. The calculation results are compared with the experimental results.

2 Experimental Methods

The experimental installation for studying the process of nucleate boiling of a dielectric liquid includes a operating chamber, a cooling system, a pressure and temperature measurement system, data collection and processing systems, a power control system and a electric heater power supply (see Fig. 1a). The operating chamber mounted on a frame. Copper-constantan thermocouples were used to measure temperature. The volumetric flow rate of water in the coolant coil of the operating chamber is measured by a rotameter and regulated by a valve. The temperature in the warming coil the

operating chamber kept constant by means of a pumping thermostat. The pressure measured using an ASG Edwards diaphragm manometer with an error of 0.2% of the total scale. The signals from the pressure gauge and thermocouples were recorded using NI equipment and processed in LabVIEW. A more complete description of the installation can be found in [6,26].

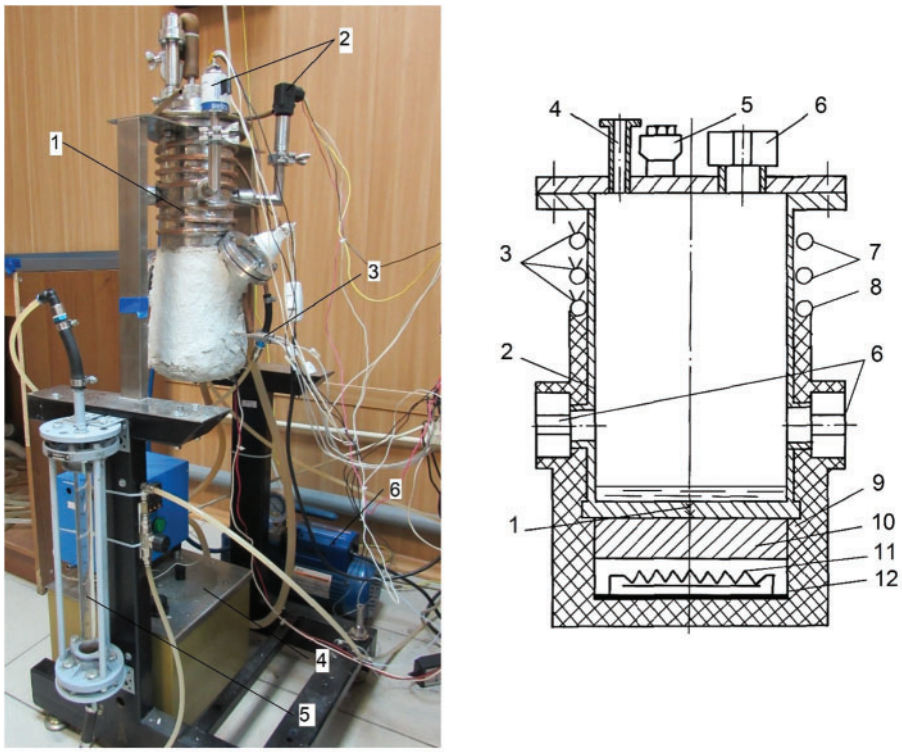

Figure 1: Experimental installation: (a)—shot of the experimental installation: 1—operating chamber of the experimental installation, 2—manometers, 3—thermocouples, 4—pumping thermostat, 5—rotameter, 6—vacuum pump; (b)—operating chamber of the experimental installation: 1—bottom, 2—casing, 3—thermocouples, 4—vacuum inlet conflate type, 5—vacuum input, 6—viewing windows, 7—coolant coil, 8—warming coil, 9—heat insulator, 10—copper plate, 11—electric resistance heater, 12—electric heater housing

The operating chamber is made of stainless steel and consists of a cylindrical casing with a wall thickness of 1 mm, a height of 300 mm and an inner diameter of $d = 120$ mm, a bottom, and a cover (Fig. 1b). An electric heater with a power of 3 kW was attached to the bottom of the chamber. A copper plate with a thickness of 30 mm is located between the heater and the bottom of the chamber. The gap between the bottom of the chamber and the copper plate is filled with a special paste with high thermal conductivity. The operant chamber was cooled by water flowing through a coolant coil on the outer surface of the upper portion of the chamber. The warming coil heated the operating chamber casing to the saturation temperature of the dielectric liquid. One window on the operating chamber casing was used for illumination. Visual observations were made through the window in the operating chamber cover and one window in the chamber casing. The results of visual observations were recorded using a video camera with a shooting frequency of 30 fps. The temperature gradient across the chamber bottom thickness was determined from readings of five copper-constantan thermocouples located at

different heights in the bottom. The heat flux through the chamber bottom to the HFE-7100 dielectric fluid was determined from the temperature gradient according to the Fourier equation. The estimated uncertainty of the heat flux measurement was nearly ~16% for $q = 10^3$ W/m^2, nearly ~10% for $q = 10^4$ W/m^2, and nearly ~4% for $q = 10^5$ W/m^2. The bottom surface temperature was determined by linear extrapolation of the measured temperature gradient. The uncertainty of bottom surface temperature measurement was no more than ~0.6°C at heat flux 10^5 W/m^2. The pressure in the operating chamber was kept constant. The lower horizontal surface (bottom) of the 12 mm thick operating chamber—a horizontal smooth surface 120 mm in diameter with roughness Rz = 3.2 μm, bounded by the vertical walls of the chamber—was used as the heating surface.

In this study dielectric liquid HFE-7100 was used as a test liquid. The experiments were carried out at a saturation pressure of 100 kPa in the operating chamber. The saturation temperature at this pressure is 61°C. The properties of the liquid and gas phases were determined using data from [28,29]. The experiments were carried out on layers with a height of $h = 1.5$; 2.5; 6; 10; 16; 25; 35 mm. The Laplace constant of HFE-7100 under the experimental conditions is 0.85 mm. The condition $d >> 3\lambda_d$ is satisfied, therefore, according to [11,12,23,24], the heating surface in these experiments can be considered as an infinite plane.

3 Results

3.1 Results of CHF Measurements and Visual Observations

In all experiments, the $q = f(T_w - T_s)$ curves were recorded, and the dependences of the heat transfer coefficient on the heat flux $\alpha = f(q)$ were constructed when processing the experimental data. The experimental data were compared with calculations using known correlations. The results were published in [30]. The results of the study of CHF depending on the layer height are shown in Fig. 2. As follows from Fig. 2, CHF first increases with an increase in the liquid layer height, reaches a maximum value at a layer height of approximately 16 mm, and then decreases. A similar dependence of CHF on the layer height was obtained in [6,7,31]. At a large layer height, CHF tends to a constant value equal to its value during pool boiling. In this case, CHF in layers of liquid with $h = 10$ mm and higher is in the range of calculated values, which are obtained in the calculation using the dependencies [13–15]. Visual observations showed that a surface drying crisis was realized in layers 1.5 and 2.5 mm high. A dry spot appeared in the center of the heating surface, which expanded from the center to the walls of the working chamber. In layers of greater height, a hydrodynamic crisis of nucleate boiling was realized. The results of CHF calculations in a 10 mm high HFE-7100 layer are published in [26]. When processing experimental data from visual observations of a layer with $h = 10$ mm in the pre-crisis mode, the distance between large bubbles that appeared on the upper boundary of the liquid layer, above the place of destruction of the "vapor jets" was measured. In layers of 16, 25 and 35 mm in height in the pre-crisis mode and after the crisis, circulation of the vapor-liquid flow was observed mainly from the center of the surface to the edges of the working chamber. Large bubbles were observed at the upper boundary of the layer, but during their movement they were carried away by the circulating flow in the horizontal direction from the point of formation, therefore layers with a height greater than 10 mm are also not considered in this work.

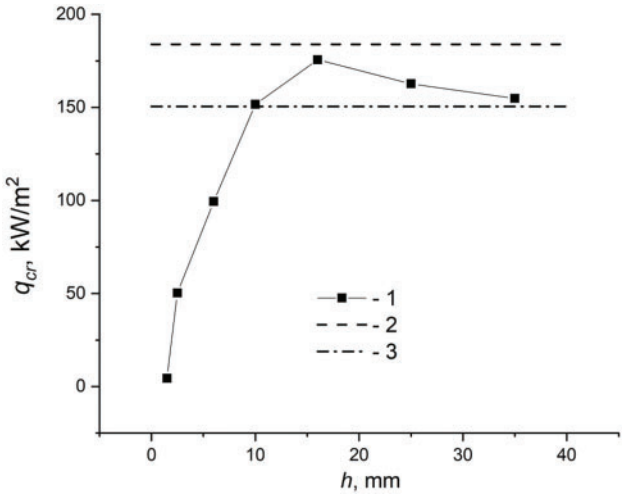

Figure 2: Dependence of CHF on the height of the liquid layer: 1—experimental data; calculated dependences: 2—[13], 3—[14,15]

This paper analyzes experimental data on the study of the hydrodynamic boiling crisis in a horizontal thin layer of dielectric liquid HFE-7100. Fig. 3 shows video footage of successive stages of the development of the crisis, indicating the moment in time from the beginning of the process when these video fragments were received. Before the crisis, the liquid layer is a fairly homogeneous bubble system (Fig. 3a). After reaching the CHF, a dry spot appeared on the heating surface. Then, near the center of the heating surface, next to the dry spot, a small region of transition boiling appeared, which is highlighted by an ellipse in Fig. 3b. Bubbles of approximately the same size are formed in the transition boiling region. Fig. 4 shows the boiling curve, and Fig. 5 shows the dependence of the change in the heating surface temperature on time. The arrows in Figs. 4 and 5 indicate the points at which the corresponding photographs shown in Fig. 3 were obtained. It is evident from Fig. 4 that the states shown in Fig. 3c,d correspond to transition boiling. The crisis develops according to a complex scenario. Upon reaching the CHF, the temperature increased with the formation of a dry spot in the center of the surface, and then, over a fairly long period of time, the structure of the layer changes, the area in it on which transition boiling exists increases, while the temperature of the heating surface remains practically constant for a sufficiently long period of time (Fig. 5).

After the area of transition boiling occupies approximately half of the heating surface (Fig. 3d), a sharp increase in temperature began (see Fig. 5). At the moment the sharp increase in temperature began, the heater was switched off.

The surface drying crisis, when a dry spot is formed on the heating surface, is typical of thin liquid layers. As follows from Fig. 2, the layer with $h = 6$ mm is in the region where the transition from boiling in thin films to pool boiling occurs. The layer with $h = 6$ mm is at the lower boundary of the transition range from CHF in thin films to CHF in a pool boiling. Judging by the observed change in the boiling crisis mechanism (Fig. 3), this is the critical height of the liquid layer $h_{cr} = 6$ mm. If $h > h_{cr}$, a hydrodynamic crisis of nucleate boiling occurs in the layer, and ordered structures are observed in the transition boiling mode. If $h < h_{cr}$, a surface drying crisis is formed in the layer.

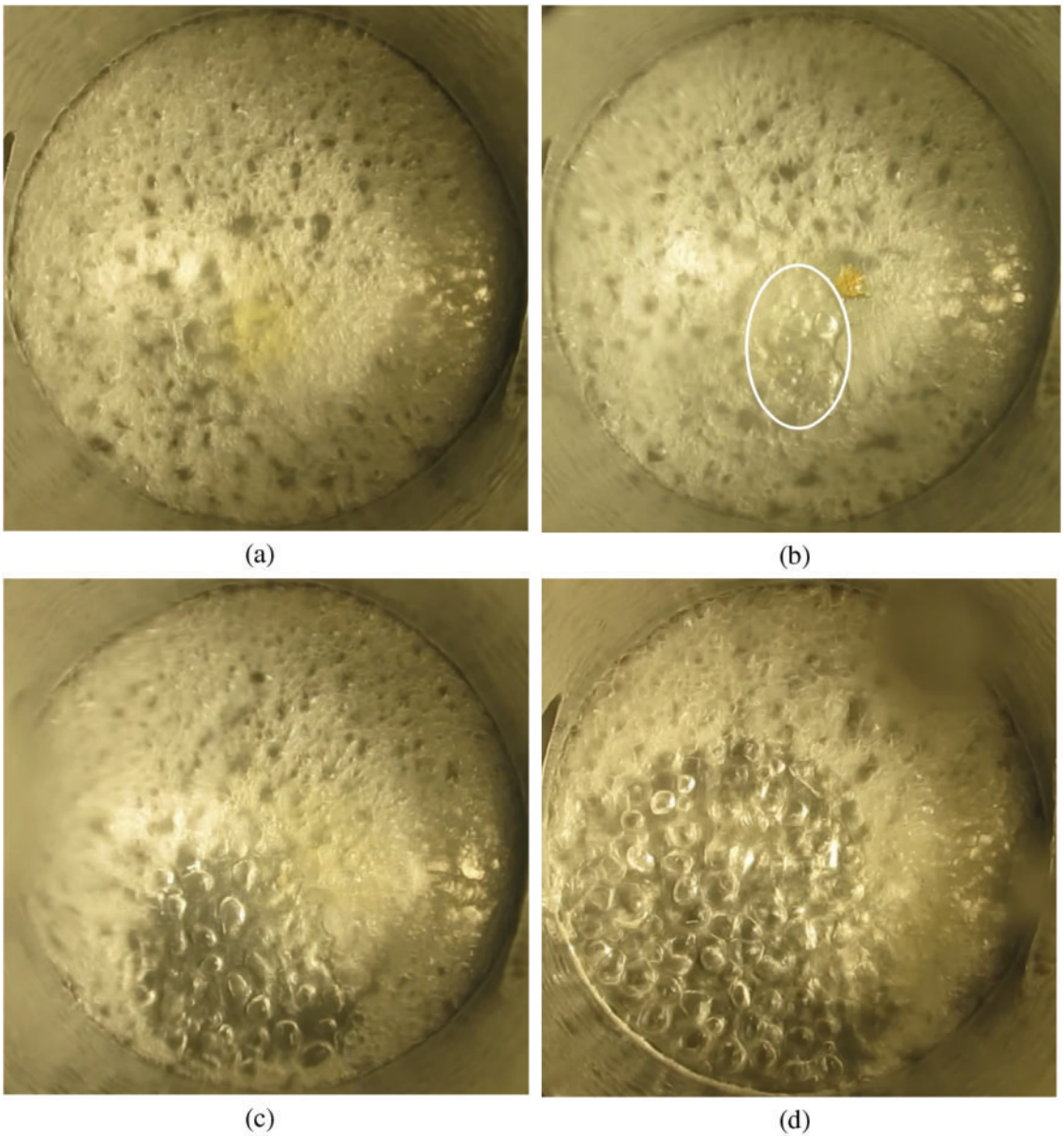

Figure 3: Development of a nucleate boiling crisis in a layer of dielectric liquid HFE-7100 at a pressure of 100 kPa. (a) pre-crisis state; (b) crisis $\tau = 0$ s; (c) transition boiling area approximately 15%, $\tau =$ 55 s; (d) transition boiling over an area of approximately 50% before the start of a sharp increase in the heating surface temperature $\tau = 1$ min 34 s

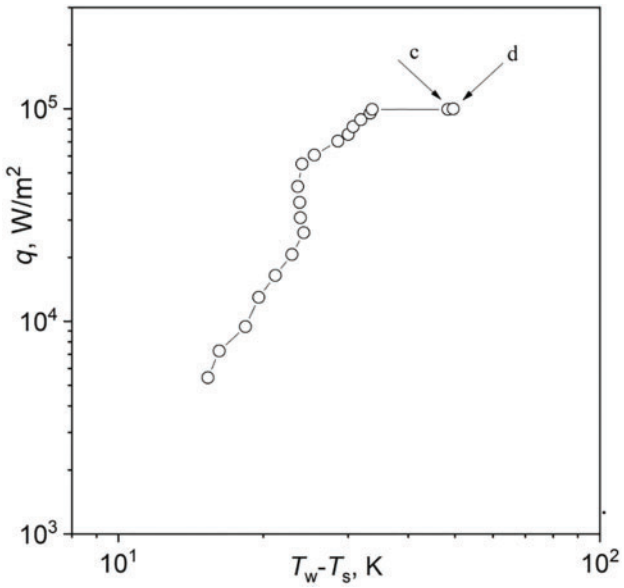

Figure 4: Boiling curve of a liquid layer with $h = 6$ mm. Lettering correspond to boiling regimes presented in Fig. 3

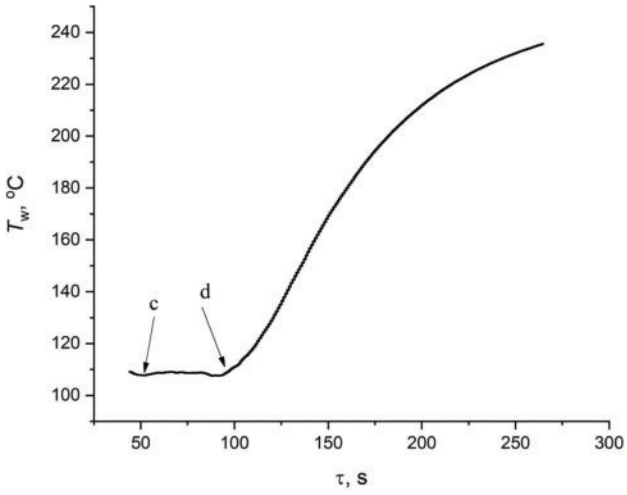

Figure 5: Change in the heating surface temperature depending on time during the development of a crisis in a layer of HFE-7100 liquid with $h = 6$ mm. Lettering correspond to boiling regimes presented in Fig. 3

Analysis of the sequence of video frames at the initial moments of time, namely in the time interval $\tau \approx 45$–55 s, that vapor bubbles form on the sides of an almost square; in Fig. 6a, they are shown as circles. Also in Fig. 6a, the arrows indicate burst bubbles, these are vapor jets. The process is almost cyclical, first bubbles form, then bursting, turning into vapor jets, and between them, in place of the burst bubbles in the previous cycle, vapor bubbles form again. The formation of bubbles and vapor jets in this regime is controlled by two-dimensional Taylor instability. This process is shown in a diagram borrowed from [27] (Fig. 6b).

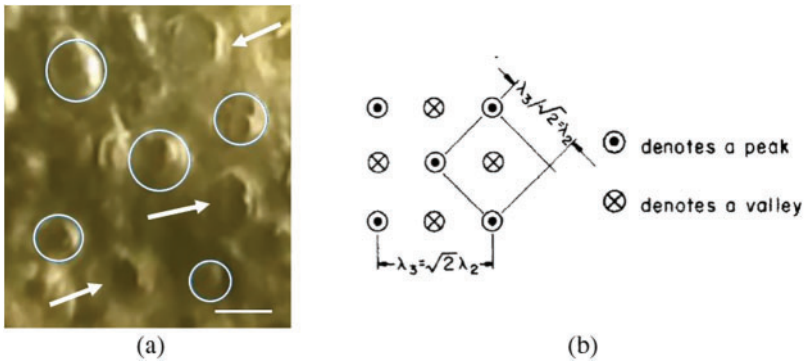

(a) (b)

Figure 6: Two-dimensional Taylor instability in a layer of liquid at the initial moment of crisis development: (a)—photograph of "vapor jets" in a thin HFE-7100 layer at nucleate boiling crisis: layer height $h = 6$ mm, volume pressure 100 kPa, $q = 96.9$ kW/m^2, temperature difference $(T_w - T_s) = 48.3$ K, scale 1 cm; (b)—top view of the liquid–vapor interface with two-dimensional Taylor instability [Adapted from "Sernas V, Lienhard JH, Dhir VK. The Taylor wave configuration during boiling from a flat plate". Int J Heat Mass Transfer. 1973;16:1820–21. Copyright 1973 Elsevier] [27]

The obtained experimental data for the transition boiling mode at times $\tau \approx 45$–55 s were processed. The results are shown in Fig. 7. During this time interval, the heat flux had already reached its critical value (Fig. 4), but the heating surface temperature remained practically constant (Fig. 5). In the process of processing the results, the diameters of the bubbles d_v and the distances between the centers of neighboring bubbles l_v were measured. More than one hundred measurements were performed for each parameter.

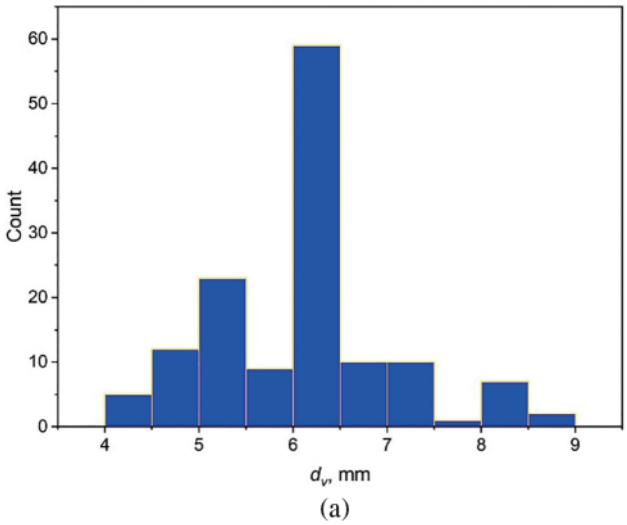

(a)

Figure 7: (Continued)

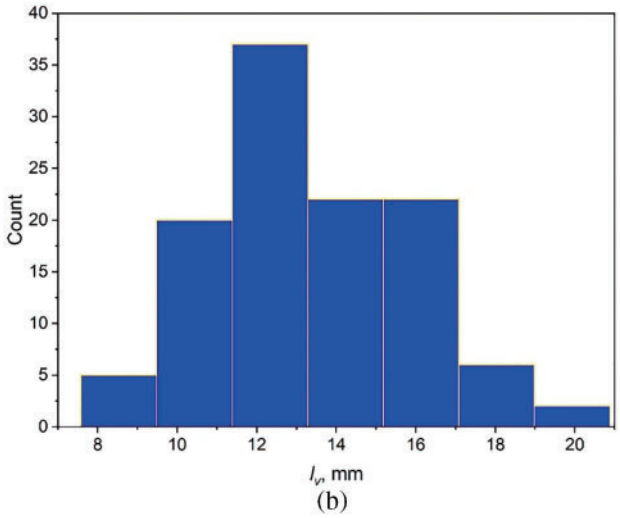

Figure 7: Histograms of the distribution of characteristic sizes during a crisis in a layer of dielectric liquid HFE-7100 with a height of $h = 6$ mm, pressure 100 kPa, $q_{cr} = 96.9$ kW/m^2, $T_w - T_s = 48.3$°C: (a) diameters of vapor bubbles, mm; (b) distance between centers of vapor bubbles, mm

When statistically processing the experimental results, size distribution histograms were constructed for each parameter, and the sample mean and standard deviation were found. Fig. 7 shows the histograms. Measured diameters of bubble d_v are plotted on the abscissa axis in Fig. 7a, and the measured distances between the centers of the vapor bubbles l_v are plotted on Fig. 7b, and the corresponding number of measurements of these quantities is shown on the ordinate axis.

The data obtained as a result of statistical processing on the sizes of bubbles and measuring the distances between them, as well as the results of measuring the CHF, are given in Table 1.

Table 1: Experimental results and calculation of characteristic linear dimensions

Pressure, kPa	T_s, °C	l_σ, mm	λ_{cr}, mm	λ_d, mm	q_{cr}, kW/m^2	d_v, mm	l_v, mm	(d_v/l_v)
100	61	0.85	5.33	9.24	96.9	6.0 ± 0.9	13.2 ± 2.6	0.45

At the onset of the crisis at a pressure of 100 kPa, the ratio (d_v/l_v) is close to that postulated by Zuber. In Fig. 6b, two instability wavelengths are highlighted, these are the one-dimensional instability wavelength $\lambda_2 = \lambda_d$ and the two-dimensional instability wavelength $\lambda_3 = \sqrt{2}\lambda_d$. In this case, the most frequently occurring wavelength seemed to be the two-dimensional instability wavelength $l_v \approx \sqrt{2}\lambda_d = 13.07$.

3.2 Comparison of CHF Calculations with Experimental Values

The obtained CHF measurement results were compared with calculations using the equation obtained as a result of the application of the mathematical apparatus developed by Zuber:

$$q_{crZ} = h_{LG}\rho_v \left(\frac{A_v}{A}\right)\left(\frac{\sigma m}{\rho_v}\right)^{1/2} \tag{2}$$

When calculating CHF using the measured parameters d_v and l_v (see Table 1) according to the classical arrangement of vapor jets at the corners of a square, the corresponding parameters were substituted into this equation. The heating surface area occupied by one vapor jet is equal to $A_v = \pi d_v^2/4$. The heating surface area on which one vapor jet is located: $A = l_v^2$. The critical Rayleigh wavelength at which vapor jets become Helmholtz unstable: $\lambda_H = 2\pi\left(\frac{d_v}{2}\right) = \pi d_v$. Critical Helmholtz wave number: $m = \frac{2\pi}{\lambda_H} = \frac{2}{d_v}$. After substituting all values, the calculation equation was obtained:

$$q_{cr.Calc} = h_{LG}\rho_v\left(\frac{\pi d_v^2}{4l_v^2}\right)\left(\frac{2\sigma}{\rho_v d_v}\right)^{1/2} \tag{3}$$

The value of the void fractions in Zuber's theory, as noted above, is equal to $\pi/16 = 0.196$. In this case, after substituting all the values, we obtain the void fraction of $\pi d_m^2/4l_v^2 = 0.162$. The experimentally observed value of the void fraction is 17% less than the theoretical value. The difference is small compared to the typical value of the void fraction at heat fluxes close to CHF, which is estimated as $\pi/4 = 0.785$.

As noted above, in the process of measuring the distance between bubbles, the length of the two-dimensional Taylor instability wave λ_3 was apparently measured most often (Fig. 6b). Theoretical instability wavelength equal to the distance between the centers of the vapor bubbles $l_{vt} = \lambda_3 = \lambda_d\sqrt{2}$. For the diameter of the vapor jet we obtain $d_{vt} = \lambda_d/\sqrt{2}$. After substituting into (3) instead of the experimentally measured values of quantities d_v and l_v their theoretical values d_{vt} and l_{vt}, we obtain an equation for calculation according to the scheme shown in Fig. 6b, where CHF is expressed in terms of λ_d:

$$q_{crt} = h_{LG}\rho_v\left(\frac{\pi}{16}\right)\left(\frac{2\sqrt{2}\sigma}{\rho_v\lambda_d}\right)^{1/2} = 0.1h_{LG}\rho_v\left(\frac{\sigma g\,(\rho_l-\rho_v)}{\rho_v^2}\right)^{1/4} \tag{4}$$

As can be seen, this equation reduces to an equation in the form of the Kutateladze Eq. (1) with a constant $k = 0.1$. A comparison of experiments with calculations is given in Table 2. The deviation from the experiment of the calculated value of the CHF was determined by the dependence:

$$\frac{|q_{cr} - q_{cr.Calc}|}{q_{cr}}100\%.$$

Table 2: A comparison of calculations with experiments

	q_{cr}	$q_{cr.Calc}$	q_{crt}	l_{vt}	d_{vt}
Parameter value	96.9 kW/m^2	99.1 kW/m^2	115 kW/m^2	13.07 mm	6.53 mm
Deviation from experiment, %		2.3	18.7	1	8.8

The deviation from the experiment of the remaining parameters indicated in Table 2 was calculated similarly, as the ratio of the modulus of the difference between the theoretical and experimental values to the experimental value.

From Table 2, it is clear that the calculated value of CHF differs from the experimentally obtained value by 2.3% if the calculation Formula (3) is used, into which the experimentally obtained values of linear dimensions d_v and l_v are substituted. The experimentally measured value of the linear dimension

l_v differs from the calculated two-dimensional wavelength of the Taylor instability $l_{vt} = \lambda_d\sqrt{2}$ by 1%, while the measured diameter of the vapor jets d_v differs from the calculated value by 8.8%, therefore the calculated CHF value using these linear dimensions differs from the experimentally determined CHF value by 18.7%.

4 Conclusion

Experimental data illustrating the effect of layer height on the CHF value during the nucleate boiling of the HFE-7100 dielectric liquid at atmospheric pressure were obtained. The CHF increased with increasing layer height up to 16 mm, and then decreased to values corresponding to the CHF during pool boiling.

The layer height influences the observed type of boiling crisis. There is a critical layer height of h_{cr}; at $h < h_{cr}$ a crisis of surface drying was observed in the layers. In layers from $h > h_{cr}$, a hydrodynamic boiling crisis was observed. In a layer with a height of $h = 6$ mm, a dry spot first formed (which is typical during a surface drying crisis). Then, regular structures in the form of large bubbles appeared on the heating surface. As a result of their destruction, "vapor jets" were generated, which are typical of transition boiling during a hydrodynamic crisis, according to Zuber's theory. The dry spot has disappeared. Such a change in the type of boiling crisis allows us to conclude that in this case $h_{cr} = 6$ mm.

Based on the results of measuring the distances between bubbles and their diameters in the transition boiling mode within a $h_{cr} = 6$ mm layer, it was found that the location of the bubbles on the heating surface, upon the destruction of which "vapor jets" are formed, is determined by the two-dimensional Taylor instability. The ratio between the diameters of the "vapor jets" and the distance between them, as well as the void fraction of the layer, practically coincides with the values postulated in Zuber's theory. In Zuber's theory, the void fraction is 0.196, while in the experiment it is 0.162. The calculation of the CHF using Zuber's mathematical apparatus aligns well with the experiment. The obtained experimental data for the critical height of the layer confirms all the main provisions of Zuber's theory.

Acknowledgement: None.

Funding Statement: This research was funded by the Russian Science Foundation, Grant No. 23-19-00245.

Author Contributions: Conceptualization, A. N. Pavlenko; validation, V. I. Zhukov; formal analysis, A. N. Pavlenko, V. I. Zhukov; investigation, V. I. Zhukov; resources, A. N. Pavlenko; writing—original draft preparation, V. I. Zhukov; writing—review and editing, A. N. Pavlenko; visualization, V. I. Zhukov; project administration, A. N. Pavlenko; funding acquisition, A. N. Pavlenko. All authors reviewed the results and approved the final version of the manuscript.

Availability of Data and Materials: Data are contained within the article.

Ethics Approval: Not applicable.

Conflicts of Interest: The authors declare no conflicts of interest to report regarding the present study.

References

1. Zhang Y, Zhao Y, Dai S, Nie B, Ma H, Li J, et al. Cooling technologies for data centres and telecommunication base stations—A comprehensive review. J Clean Prod. 2022;334:130280. doi:10.1016/j.jclepro.2021.130280.
2. Sajjad U, Sadeghianjahromi A, Ali HM, Wang C-C. Enhanced pool boiling of dielectric and highly wetting liquids-a review on enhancement mechanisms. Int Commun Heat Mass Transfer. 2020;119:104950. doi:10.1016/j.icheatmasstransfer.2020.104950.
3. Alvariño PF, Simón MLS, Guzella MS, Paz JMA, Jabardo JMS, Gómez LC. Experimental investigation of the CHF of HFE-7100 under pool boiling conditions on differently roughened surfaces. Int J Heat Mass Transfer. 2019;139(2):269–79. doi:10.1016/j.ijheatmasstransfer.2019.04.142.
4. Fan X, Gu S, Lei J, Luo G, Meng F, Wu L, et al. Experimental and analytical study on the influence of saturation pressure and surface roughness on pool boiling CHF of HFE-7100. Int J Chem Eng. 2022;2022(1):1–18. doi:10.1155/2022/4875208.
5. Yu J, Chen Z, Utaka Y. Critical heat flux characteristics in pool boiling at low pressure for dielectric fluid Novec 7100. Int J Heat Mass Transfer. 2024;232(11):125959. doi:10.1016/j.ijheatmasstransfer.2024.125959.
6. Zhukov VI, Pavlenko AN. Heat transfer and critical phenomena during evaporation and boiling in a thin horizontal liquid layer at low pressures. Int J Heat Mass Transfer. 2018;117(11):978–90. doi:10.1016/j.ijheatmasstransfer.2017.10.060.
7. Pavlenko AN, Zhukov VI, Shvetsov DA. Crisis phenomena and heat-transfer enhancement during boiling and evaporation in horizontal liquid films (Review). Therm Eng. 2022;69(11):886–901. doi:10.1134/S0040601522110076.
8. Wang X, Tang Y, Liu L, Zhang P, Zhang Y, Zhao J, et al. Influence of smooth heater size on critical heat flux and heat transfer coefficient of saturated pool boiling heat transfer. Exp Therm Fluid Sci. 2024;151(8):111068. doi:10.1016/j.expthermflusci.2023.111068.
9. Taylor GI. The instability of liquid surfaces when accelerated in a direction perpendicular to their plane. Proc Roy Soc London Series A. 1950;201(1065):192–96. doi:10.1098/rspa.1950.0052.
10. Bellman R, Pennington RH. Effects of surface tension and viscosity on Taylor instability. Quart Appl Math. 1954;12(2):151–62. doi:10.1090/qam/63198.
11. Lienhard JH, Dhir VK. Hydrodynamic prediction of peak pool-boiling heat fluxes from finite bodies. Trans ASME J Heat Transfer. 1973;95:152–58.
12. Lienhard JH, Dhir VK. Extended hydrodynamic theory of the peak and minimum pool boiling heat fluxes. Lexington: University of Kentucky; 1973. NASA CR-2270.
13. Kutateladze SS. Hydrodynamic model of heat transfer crisis in free-convection boiling. J Tech Phys. 1950;20(11):1389–92.
14. Zuber N. On the stability of boiling heat transfer. ASME J Heat Transfer. 1958;80(2):711–20.
15. Zuber N. Hydrodynamic aspects of boiling heat transfer (Ph.D. Thesis). Ramo-Wooldridge Corp.; Univ. of California, Los Angeles, CA, USA; 1959.
16. Liang G, Mudawar I. Pool boiling critical heat flux (CHF)—Part 1: review of mechanisms, models, and correlations. Int J Heat Mass Transfer. 2018;117:1352–67.
17. Liang G, Mudawar I. Pool boiling critical heat flux (CHF)—Part 2: assessment of models and correlations. Int J Heat Mass Transfer. 2018;117:1368–83.
18. Patel R, Meyer M, Hartwig J, Mudawar I. Review of cryogenic pool boiling critical heat flux databases, assessment of models and correlations, and development of new universal correlations. Int J Heat Mass Transfer. 2022;190:122579.
19. Xiang L, Song Y, Yang D, Zhang Z, Yao S, Vafai K. Boiling mechanism of biphilic surfaces based on Helmholtz instability and Taylor instability. Int J Multiphase Flow. 2024;173:104735.

20. Lienhard JH. Snares of pool boiling research: putting our history to use. In: Proceedings of the 10th International Heat Transfer Conference, 1994; Brighton, UK; p. 333–48.
21. Yagov VV. Is a crisis in pool boiling actually a hydrodynamic phenomenon? Int J Heat Mass Transfer. 2014;73:265–73.
22. Bergles AE. What is a real mechanism of CHF in pool boiling? In: Dhir VK, Bergles AE, editors. Pool and external flow boiling. New York: ASME; 1992. p. 165–70.
23. Theofanous TG, Tu JP, Dinh AT, Dinh TN. The boiling crisis phenomenon: part I: nucleation and nucleate boiling heat transfer. Exp Therm Fluid Sci. 2002;26:775–92.
24. Theofanous TG, Tu JP, Dinh AT, Dinh TN. The boiling crisis phenomenon: part II: dryout dynamics and burnout. Exp Therm Fluid Sci. 2002;26:793–810.
25. Zhukov VI, Pavlenko AN. Crisis of nucleate boiling in a finite-height horizontal layer of liquid. J Engin Thermophys. 2020;29(1):1–13. doi:10.1134/S1810232820010014.
26. Zhukov VI, Pavlenko AN. Symmetry of structures under two-dimensional instability in a finite-height horizontal layer of boiling liquid. Symmetry. 2023;15(9):1792. doi:10.3390/sym15091792.
27. Sernas V, Lienhard JH, Dhir VK. The Taylor wave configuration during boiling from a flat plate. Int J Heat Mass Transfer. 1973;16(9):1820–21. doi:10.1016/0017-9310(73)90175-0.
28. 3M™ Novec™ Engineered Fluid HFE-7100 Datasheet. Available from: https://www.sil7mid.com/getattachment/706d712f-db18-4563-bcd6-ab78cba39349/3M-Novec-HFE-7100-TDS.aspx. [Accessed 2018].
29. Rausch MH, Kretschmer L, Will S, Leipertz A, FroÏba AP. Density, surface tension, and kinematic viscosity of hydrofluoroethers HFE-7000, HFE-7100, HFE-7200, HFE-7300, and HFE-7500. J Chem Eng Data. 2015;60:3759–65.
30. Shvetsov DA, Pavlenko AN, Zhukov VI. Heat transfer during boiling in horizontal layers of HFE-7100 on smooth and modified surfaces. J Eng Thermophys. 2024;33(2):250–68. doi:10.1134/S1810232824020024.
31. Shukla MY, Kandlikar SG. Influence of liquid height on bubble coalescence, vapor venting, liquid return, and heat transfer in pool boiling. Int J Heat Mass Transf. 2021;173(12):121261. doi:10.1016/j.ijheatmasstransfer.2021.121261.